www.czasopisma.pan.pl PAN POLSKA AKADEMIA NAUK www.journals.pan.pl

Arch. Metall. Mater. **68** (2023), 1, 71-75

DOI: https://doi.org/10.24425/amm.2023.141474

GWANGHUN KIM[1], JUNGBIN PARK[1], SEOK-JAE LEE[1], HEE-SOO KIM[2*]

MICROSTRUCTURE AND HARDNESS OF Cu-22Sn-xC ALLOYS FABRICATED BY POWDER METALLURGY

Cu-Sn alloys have been known as bronze since ancient times and widely used as electrode materials, ornaments, tableware and musical instruments. Cu-22Sn alloy fabrication by hot forging process is a Korean traditional forged high-tin bronze. The tin content is 22 percent, which is more than twice that of bronze ware traditionally used in China and the West. Copper and tin have a carbon solubility of several ppm at room temperature, making Cu-Sn-C alloys difficult to manufacture by conventional casting methods. Research on the production of carbon-added copper alloys has used a manufacturing method that is different from the conventional casting method. In this study, Cu-22Sn-xC alloy was fabricated by mechanical alloying and spark plasma sintering. The carbon solubility was confirmed in Cu-Sn alloy through mechanical alloying. The lattice parameter increased from A0 to C2, and then decreased from C4. The microstructural characteristics of sintered alloys were determined using X-ray diffraction and microscopic analysis. As a result of comparing the hardness of Cu-22Sn alloys manufactured by conventional rolling, casting, and forging and Cu-22Sn-xC alloy by sintered powder metallugy, B0 sintered alloy was the highest at about 110.9 HRB.

Keywords: Cu-Sn alloy; Nanocrystalline; Carbon solubility; Mechanical alloying

1. Introduction

Cu-Sn alloys have been known as “bronze” since ancient times. They have been widely used as electrode materials, weapons, ornaments, tableware and musical instruments because of their high strength, high impact resistance, and good corrosion resistance [1-3]. The Sn content varies according to the application. In particular, Cu-22Sn alloy manufactured by hot processing is a traditional Korean high-tin bronze. Since in metallurgy, to make a quality alloy of copper and tin, the proportion of tin must be less than 10%, because by increasing its proportion, it is more difficult to make bronze. However, the Korean traditional forged high-tin bronze, allowing the strength of materials through molding, even if the proportion of tin is increased to 22 wt.%.

Carbon is the most effective element for increasing hardness and strength in Fe-based alloys. It can be thought that the addition of carbon contributes to the hardening of Cu-Sn alloys. However, copper and tin have a carbon solubility of several ppm at room temperature, making it difficult to manufacture Cu-Sn-C alloys by conventional casting methods [4,5]. Consequently, research on the production of carbon-added copper alloys has employed a manufacturing method that is different from the conventional casting method.

Powder metallurgy is a bottom-up manufacturing method that can overcome the limitations of crystal grain refinement process by cold rolling and recrystallization of cast and forged bulk materials [6-8]. Mechanical alloying (MA) in powder metallurgy is performed by mixing amorphous alloy, metal, nanocomposite powders using a high-energy ball mill, through which nanostructured alloys and compounds are easily manufactured [9,10]. Saji et al. [11] and Yamane et al. [12] prepared Cu-C supersaturated solid solution using an attrition mill and planetary mill. Saji et al. [11] reported that the supersaturated solute carbon atoms occupy the interstitial positions in the face-centered cubic (fcc) α-Cu solid solution, resulting in expansion of the lattice parameter of the α-Cu. High-energy ball milling increases the solid solubility limit and is used for alloying of low solubility or immiscible systems such as Cu-Cr, Cu-Nb, and Cu-C alloys [13-16]. However, studies on the addition of carbon to Cu-Sn alloys with high tin contents are insufficient.

In this study, a Cu-22Sn alloy with added carbon was manufactured through the MA and a rapid sintering process. The variation in the characteristics according to the amount of added carbon were determined using X-ray diffraction (XRD) and microscopic analysis. The hardness of cast and forged Cu-22Sn alloys was compared with that of Cu-22Sn-xC sintered alloys.

[1] JEONBUK NATIONAL UNIVERSITY, DIVISION OF ADVANCED MATERIALS ENGINEERING, 567 BAEKJE-DAERO, DEOKJIN-GU, JEONJU 54896, REPUBLIC OF KOREA
[2] CHOSUN UNIVERSITY, DEPARTMENT OF MATERIALS SCIENCE AND ENGINEERING, 309 PILMUN-DAERO, DONG-GU, GWANGJU 61452, REPUBLIC OF KOREA

* Corresponding author: heesoo@chosun.ac.kr

The effects of the milling time and amount of added carbon on the microstructure and mechanical properties of Cu-22Sn alloys were investigated.

2. Experimental procedure

Cu powder (Alfa Aesar, Korea) with a purity of 99.9% and an average particle size (APS) of < 44~149 μm, tin powder (Alfa Aesar, Korea) with a purity of 99.8% and APS of < 44 μm and graphite powder (Alfa Aesar, Korea) with a purity of 99% and APS of < 7~11 μm were used. MA was performed using a high-energy ball mill (FRITSCH, Pulverisette-6) to produce nanocrystalline Cu-22Sn-xC (wt.%) alloy powder. Cylindrical SKD-11 tool steel jar and FeCrC balls with a diameter of 10 mm were used for milling. The ratio of balls to powder was set to 30:1 and 1.0 wt.% stearic acid (Alfa Aesar, $CH_3(CH_2)_{16}CO_2H$) was added as a process control agent to balance cold welding and fracture. The ball milling was carried out in pure Ar atmosphere at 250 rpm for 6 h and 24 h, and the notations and corresponding conditions (milling time and carbon addition amounts) are shown in Table 1. A graphite mold with an inner diameter of 10 mm, an outer diameter of 35 mm, and a height of 40 mm was filled with the milled alloy powder prepared by MA, which was rapidly sintered by spark plasma sintering (SPS). The sintering conditions were heated to 400 °C at a heating rate of 1 °C/s under high vacuum and uniaxial pressure of 80 MPa, where it was maintained for 15 min before being cooled in furnace and air. The relative density of the sintered alloy was measured using the Archimedes method. The phase analysis and structural properties of the powder including grain size and lattice parameters were analyzed using XRD (Shimadzu, XRD-6100) with a Cu Kα target and a scan speed of 2 °/min at 40 kV and 30 mA. The mechanical properties of the sintered alloys were measured using a Rockwell hardness tester (SSAUL BESTECH, BESTROC-300N). The microstructures of the sintered alloys were observed using optical microscopy (OM, Leica, DMC 2900) and scanning electron microscopy (SEM, JSM-7100 F, JEOL). The chemical composition of each microstructure was analyzed using energy-dispersive X-ray spectroscopy (EDS, JSM-7100 F, JEOL).

TABLE 1

Chemical composition of the Cu-22Sn-xC alloys with milling time

Notation	Composition (wt.%)			Composition (at.%)			Mechanical milling time (h)
	Cu	Sn	C	Cu	Sn	C	
A0	78	22	0	86.88	13.12	0	6
B0	78	22	0	86.88	13.12	0	24
C2	76	22	2	77.72	11.73	10.54	24
C4	74	22	4	70.31	10.62	19.08	24
C6	72	22	6	64.19	9.69	26.12	24

3. Results and discussion

Fig. 1 shows the XRD patterns of Cu-Sn-xC alloy powder manufactured under for each condition using a high-energy ball mill. In A0 with a milling time of 6 h, MA was incomplete and Cu and η-Cu_6Sn_5 phases were observed. Only the β-$Cu_{17}Sn_3$ phase was observed in B0 with a milling time of 24 h. In C2

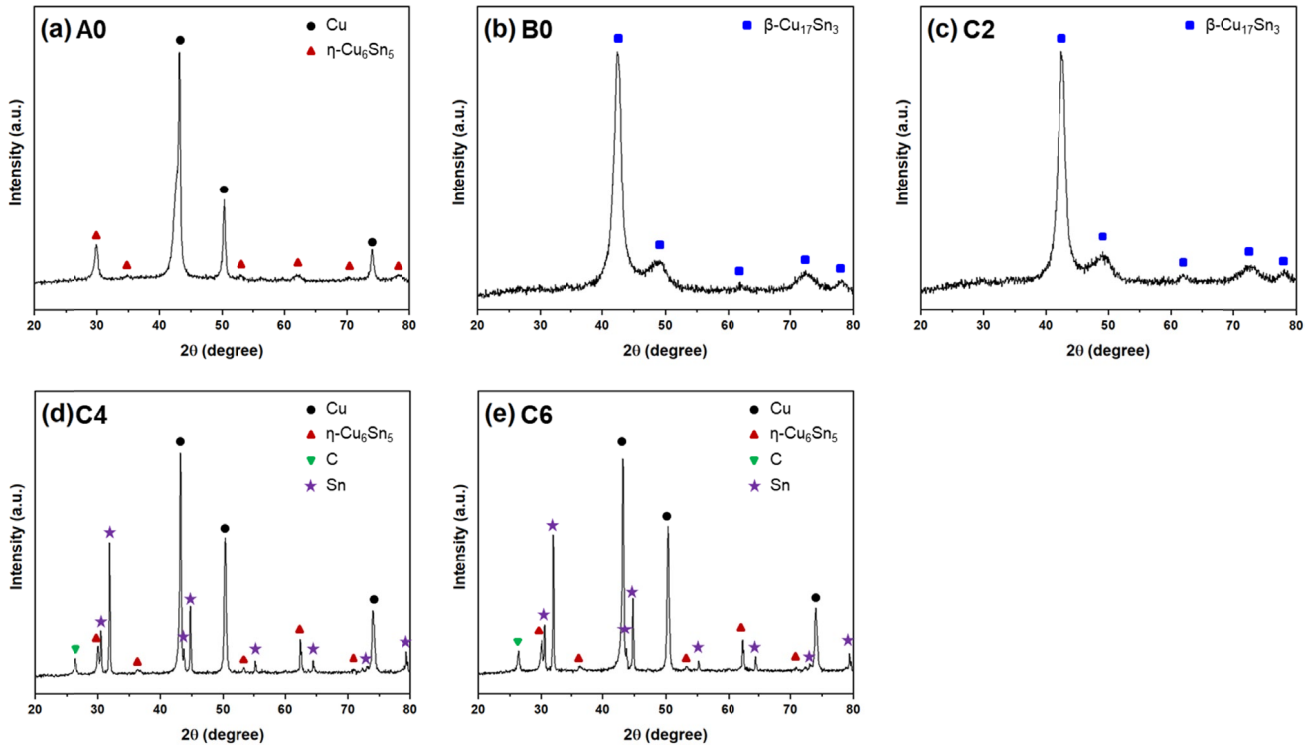

Fig. 1. XRD patterns of the milled Cu-22Sn-xC powders after different milling time and chemical composition. (a) A0 with 6 h, (b) B0 with 24 h, (c) C2 with 6 h, (d) C4 with 6 h and (e) C6 with 6 h

with 2 wt.% of added carbon, the β-$Cu_{17}Sn_3$ phase was observed because carbon was dissolved in the matrix. It was confirmed that B0 and C2 were mechanically alloyed. C4 and C6 with high carbon content were observed with Cu, Sn, C, and η-Cu_6Sn_5 phases were observed. Carbon interfered with the welding and agglomeration of powders, making MA difficult, and there was residual carbon because carbon solubility is saturated [17].

Fig. 2 shows results of the lattice parameters of the milled alloy powders according to the carbon content. The lattice parameter increased from A0 to C2 and decreases after C4. As the milling time increased, the lattice parameter of B0 increased with the increased milling time because of the formation of β-$Cu_{17}Sn_3$ phase, and the lattice parameter of C2 increased because of carbon solid solution in the lattice. When more than 4 wt.% of carbon is added, residual carbon was generated, which interfered with MA. Therefore, the lattice parameter decreased owing to the formation of Cu phase.

Cu-Sn-xC alloy powder samples were manufactured by MA and SPS. The relative densities of the sintered alloys were measured using the Archimedes method, and relative densities were calculated using theoretical density and measured densities. The relative densities of A0, B0, C2, C4 and C6 were 97.4, 97.5, 99.7, 97.6 and 96.9 %, respectively, and measured relative densities of the samples were close to the theoretical densities owing to densification during SPS. Fig. 3 shows the XRD patterns of the sintered Cu-Sn-xC alloys. Cu and δ-$Cu_{41}Sn_{11}$ phases were observed in A0, B0 and C2, while Cu, Sn, C and ε-Cu_3Sn phases were observed in C4 and C6. It was confirmed that changed as the intermetallic phase and residual carbon occurred as the carbon content increased. The residual carbon atoms exist in the

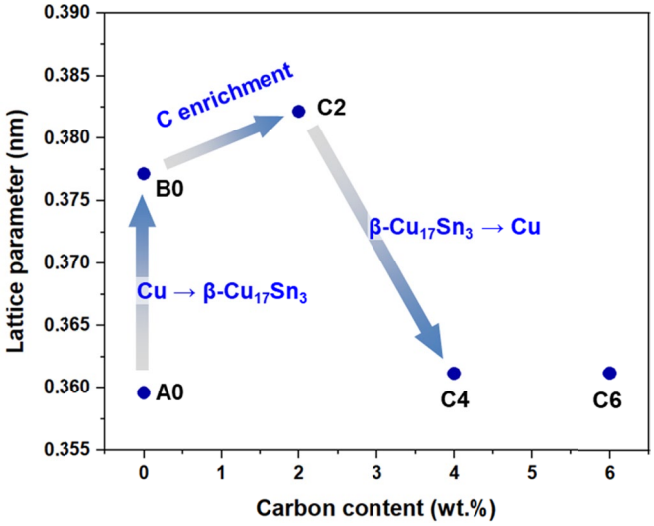

Fig. 2. Variation of the lattice parameter of Cu with carbon content. The lattice parameter increased from A0 to C2 and decreased after C4

form of amorphous carbon for C4 and C6, respectively. In C4 and C6, the η-Cu_6Sn_5 phase decomposed by thermal diffusion during sintering, thereby forming ε-Cu_3Sn [18]. The crystallite sizes of sintered alloys were calculated by the Williamson-Hall equation (Eq. (1)) using the Bragg angle and the full width at half maximum (FWHM) of the XRD peak [19].

$$\beta_r \cos\theta = \frac{k \cdot \lambda}{D} + \eta \sin\theta \tag{1}$$

where β_γ is the FWHM of XRD peak, θ is the Bragg angle, λ is the wavelength of the Cu K_α source, κ is a constant, D is the

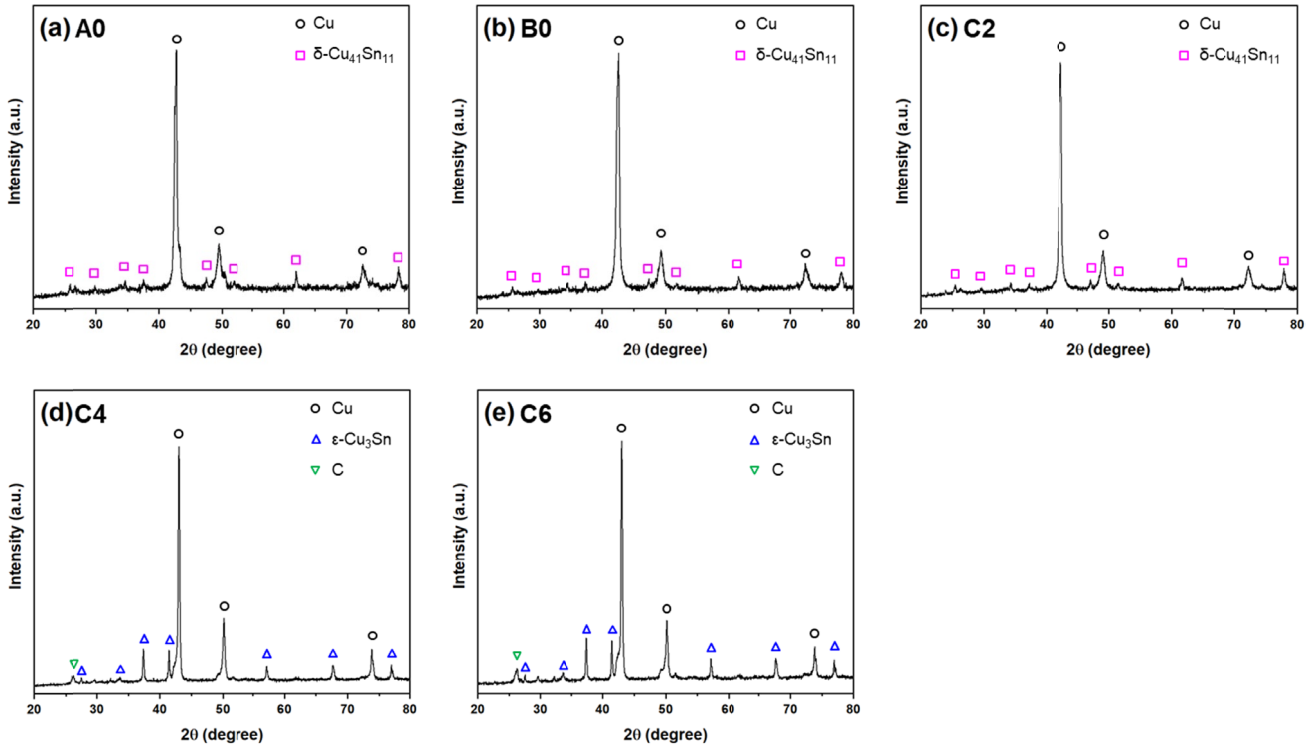

Fig. 3. XRD patterns of the sintered Cu-22Sn-xC alloys after different milling time and chemical composition. (a) A0 with 6 h, (b) B0 with 24 h, (c) C2 with 6 h, (d) C4 with 6 h and (e) C6 with 6 h

crystallite size and η is the lattice strain. The crystallite sizes of the sintered Cu-Sn-xC alloys A0-C6 were approximately 43.8, 20.9, 38.8, 88.8 and 67.6 nm, respectively.

The OM and SEM images and EDS analysis results are shown in Fig. 4. Fig. 4(a) shows the OM image of Cu-Sn-xC alloys for A0-C6. Cu and δ-$Cu_{41}Sn_{11}$ phases were observed in A0-C2, while Cu, Sn, C, and ε-Cu_3Sn phases were observed in C4 and C6 [20]. Fig. 4(b) shows the results of SEM images and EDS point analysis used to distinguish the Cu_x-Sn_{100-x} intermetallic phases of C2 and C6. The Cu_x-Sn_{100-x} intermetallic phase was calculated by excluding the carbon content related to the solid solubility of carbon by MA. As a result of EDS point analysis, it was confirmed that the δ-$Cu_{41}Sn_{11}$ phase appeared in C2, and the ε-Cu_3Sn phase with residual carbon in the black region were confirmed in C6.

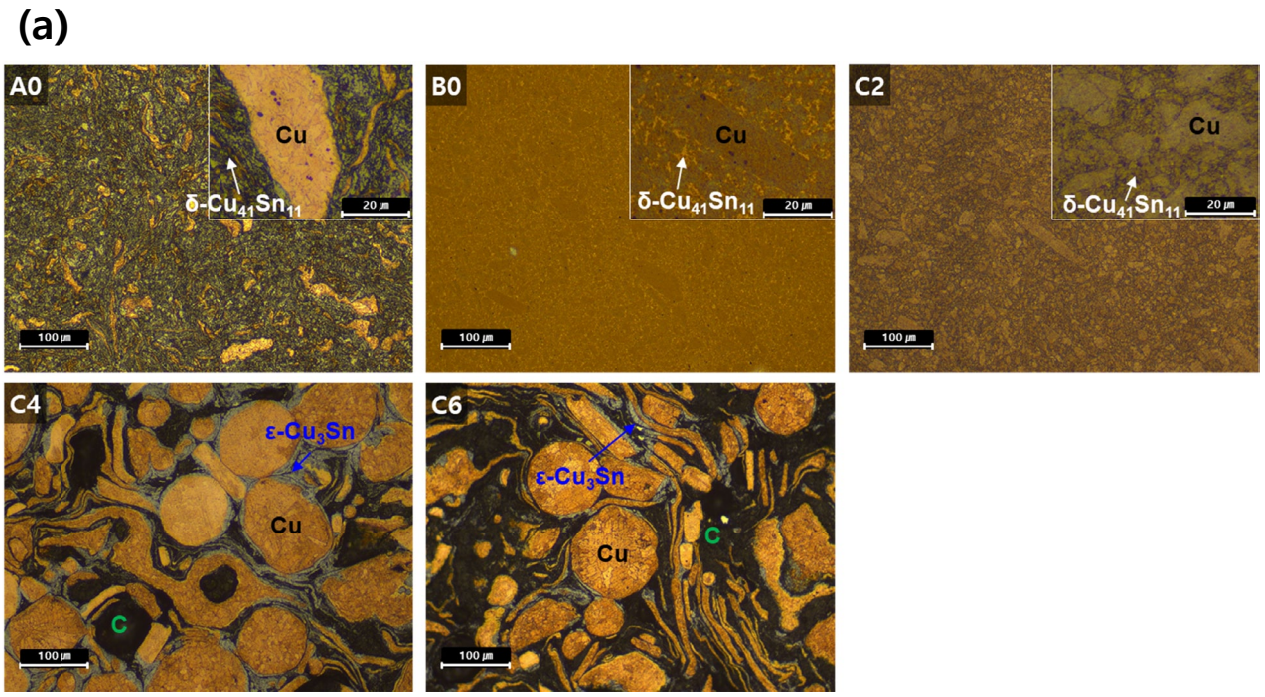

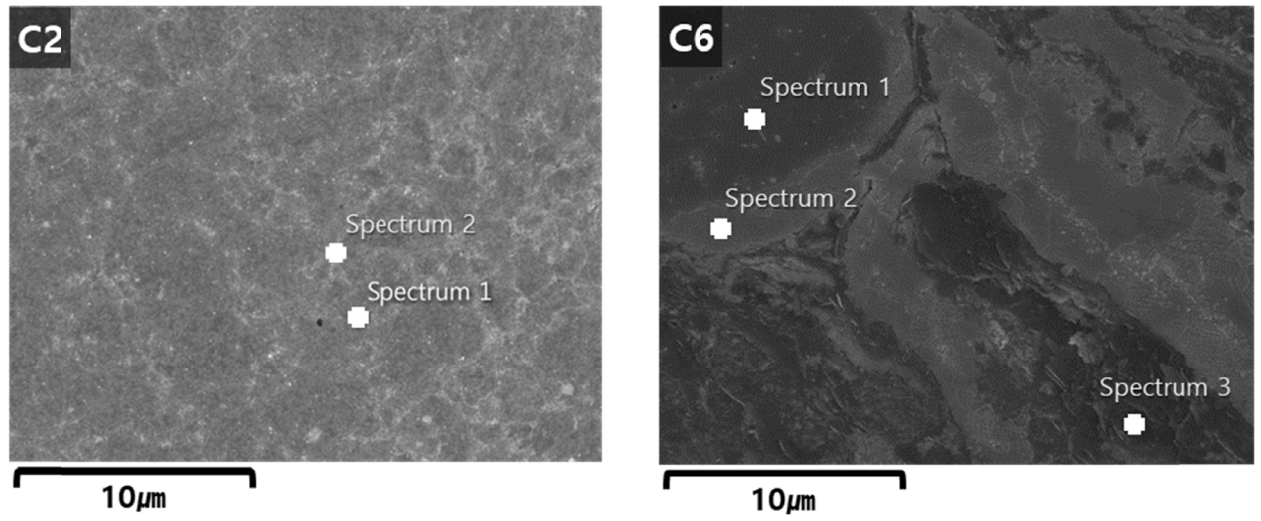

Element	Spectrum 1	Spectrum 2
	Wt.%	Wt.%
C	7.81 ± 1.03	9.42 ± 1.00
Cu	82.37 ± 1.09	65.16± 2.03
Sn	9.82 ± 0.92	25.32 ± 1.03
Total:	100.00	100.00

Element	Spectrum 1	Spectrum 2	Spectrum 3
	Wt.%	Wt.%	Wt.%
C	8.47 ± 1.48	6.77 ± 0.81	84.40 ± 3.24
Cu	86.59 ± 1.57	58.07 ± 2.61	2.96 ± 0.84
Sn	4.94 ± 1.01	35.16 ± 3.32	12.64 ± 2.60
Total:	100.00	100.00	100.00

Fig. 4. Microstructure analysis of the sintered Cu-22Sn-xC alloys. (a) Optical microscope images (×200) of Cu-22Sn-xC alloys. The inset shows the high resolution image (×1000) of A0, B0 and C2, respectively. (b) SEM (×5000) and EDS analysis results of C2 and C6

Fig. 5 shows the hardness of Cu-22Sn alloys manufactured by rolling, casting and forging, and the hardness of Cu-22Sn-xC sintered alloys. Sintered alloy B0 had the highest hardness owing to the influence of the δ-$Cu_{41}Sn_{11}$ phase, which improves the strength and hardness, and the Hall-Petch effect due to grain refinement [21-23]. A higher the interconnection between the Cu and Sn particles provides higher the mechanical interlocks in these alloys. However, increasing the carbon content weakens the interlocks, leading to a decrease in hardness [24]. Consequently, it is confirmed that C4 and C6 with high carbon contents fractured during hardness test owing to the brittleness of the intermetallic phase.

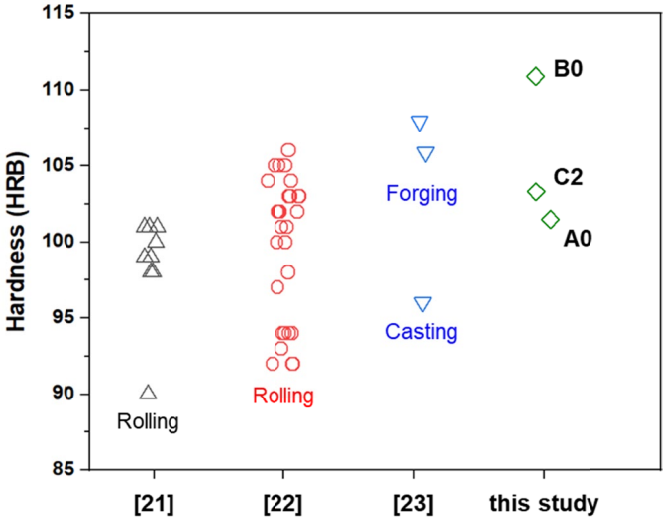

Fig. 5. Comparison of hardness value between Cu-22Sn alloys manufactured by conventional rolling, casting, and forging and the sintered Cu-22Sn-xC alloys

4. Conclusions

In this study, nanocrystalline Cu-22Sn-xC alloys according to the milling times and added carbon were manufactured using a high-energy ball milling and SPS. Carbon solubility was confirmed in Cu-Sn alloy through MA. For the alloy powder, the lattice parameter increased from A0 to C2 owing to β-$Cu_{17}Sn_3$ phase formation and carbon solid solution, and the lattice parameter decreased owing to the formation of Cu phase in C4 with a high carbon content. The microstructural characteristics of the sintered Cu-22Sn-xC alloys were analyzed by XRD, OM, SEM and EDS analysis to determine the differences according to milling time and carbon content. The hardness of Cu-22Sn alloys manufactured by conventional rolling, casting, and forging were compared with those of the sintered Cu-22Sn-xC alloys. The B0 sintered alloy had the highest hardness owing to the Hall-Petch effect and the δ-$Cu_{41}Sn_{11}$ phase, which affects strength and hardness. C4 and C6 had high carbon contents, which weakened the interlock, lowered the hardness, and caused fractured during measurement owing to the brittleness of the intermetallic phase.

Acknowledgments

This research was supported by the Traditional Culture Convergence Research Program through the National Research Foundation of Korea (NRF) funded by the Ministry of Science, ICT and Future Planning (2017M3C1B5018726).

REFERENCES

[1] J.X. Hou, W Zhou, S.H. Zhang, S.Y. Hou, M.Q. Sheng, Int. J. Electrochem. Sci. **10**, 8558 (2015).
[2] S. Ozel, F.A. Celik, M. Kaya, Phys. Lett. A **384**, 126418 (2020).
[3] Yu. K. Frvstov, L.V. Zhuravel, L.P. Kochetkova, Met. Sci. Heat Treat. **45**, 16 (2003).
[4] G.A. Lopez, E.J. Mittemeijer, Scr. Mater. **51**, 1 (2004).
[5] T. Yamane, H. Okubo, N. Oki, K. Hisayuki, M. Kiritani, M. Komatsu, Mater. Sci. Eng. A **350**, 173 (2003).
[6] J.S. Benjamin, T.E. Volin, Metall. Trans. **5**, 1929 (1974).
[7] G. Kim, J. Jeon, N. Seo, S. Choi, M.S. Oh, S.B. Son, S.J. Lee, Arch. Metall. Mater. **66**, 759 (2021).
[8] S.J. Lee, S. Lee, B.C. De Cooman, Scr. Mater. **64**, 649 (2011).
[9] J. Jeon, S. Choi, N. Seo, Y.H. Moon, I.J. Shon, S.J. Lee, Arch. Metall. Mater. **65**, 1249 (2020).
[10] C. Suryanarayana, Research, 17 (2019).
[11] S. Saji, T. Kadokura, H. Anada, K. Notoya, N. Takano, Mater. Trans. JIM **39**, 778 (1998).
[12] K.B. Gerasimov, S.V. Mytnichenko, S.V. Pavlov, Dokl. Phys. Chem. **351**, 310 (1996)
[13] T. Yamane, H. Okubo, N. Oki, K. Hisayuki, M. Konishi, Y. Minamino, Y. Koizumi, M. Kiritani, M. Komatsu, S.J. Kim, J. Jpn. Soc. Powder. Powder. Metall. **48**, 9 (2001).
[14] E. Botcharova, M. Heilmaier, J. Freudenberger, G. Drew, D. Kudashow, U. Martin, L. Schultz, J. Alloys Compd. **351**, 119 (2003).
[15] M.T. Marques, J.B. Correia, O. Conde, Scr. Mater. **50**, 963 (2004).
[16] W. Zeng, D.S. Zhou, D. Zhang, X. Li, Mater. Res. **18**, 152 (2015).
[17] X. Liu, Y. Liu, X. Ran, J. An, Z. Cao, Mater. Charact. **58**, 504 (2007).
[18] Y.S. Kim, J.H, Kwon, D.Y. Yoo, S.K. Park, D.J. Lee, D.G. Lee, J. Kor. Inst. Met. Mater. **55**, 165 (2017).
[19] N. Ser, G. Kim, S. Choi, J. Jeon, M.S. Oh, S.B. Son, S.J. Lee, Powder. Metall. **64**, 1 (2021).
[20] J.Y. Yang, W.J. Kim, J. Mater. Res. Technol. **9**, 749 (2020).
[21] Z. Mao, D.Z. Zhang, J. Jiang, G. Fu, P. Zhang, Mater. Sci. Eng. A **721**, 125 (2018).
[22] P. Han, F.R. Xiao, W.J. Zou, B. Liao, Mater. Des. **53**, 38 (2014).
[23] S.M. So, K.Y. Kim, S.J. Lee, Y.J. Yu, H.A. Lim, M.S. Oh, Mater. Sci. Eng. A **796**, 140054 (2020).
[24] A. Nassef, M.E. Hadek, Adv. Mater. Sci. Eng. **2016**, 1 (2016).